

Ultra-Flattened Normal Dispersion Fiber for Supercontinuum and Dissipative Soliton Resonance Generation at $2 \mu\text{m}$

Volume 11, Number 3, June 2019

Tianye Huang, *Member, IEEE*

Qian Wei

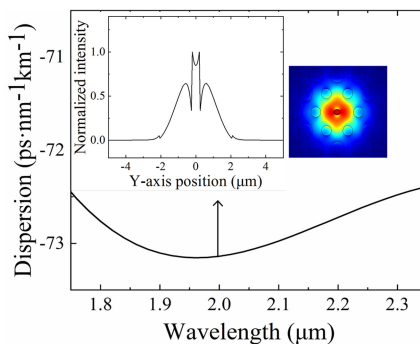
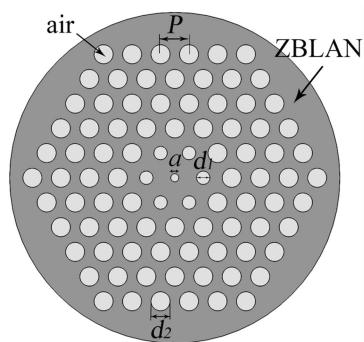
Zhichao Wu

Xu Wu

Pan Huang

Zhuo Cheng


Perry Ping Shum, *Senior Member, IEEE*



DOI: 10.1109/JPHOT.2019.2915265

1943-0655 © 2019 IEEE

Ultra-Flattened Normal Dispersion Fiber for Supercontinuum and Dissipative Soliton Resonance Generation at 2 μm

Tianye Huang ^{1,2} *Member, IEEE*, Qian Wei,¹ Zhichao Wu,³ Xu Wu,¹
Pan Huang,¹ Zhuo Cheng,¹
and Perry Ping Shum,⁴ *Senior Member, IEEE*

¹School of Mechanical Engineering and Electronic Information, China University of Geosciences, Wuhan 430074, China

²Hubei Key Laboratory of Inland Shipping Technology, Wuhan 430063, China

³National Engineering Laboratory for Next Generation Internet Access System, School of Optics and Electronic Information, Huazhong University of Science and Technology, Wuhan 430074, China

⁴Center of Fiber Technology, School of Electrical and Electronic Engineering, Nanyang Technological University, Singapore 639798

DOI:10.1109/JPHOT.2019.2915265

1943-0655 © 2019 IEEE. Translations and content mining are permitted for academic research only.

Personal use is also permitted, but republication/redistribution requires IEEE permission.

See http://www.ieee.org/publications_standards/publications/rights/index.html for more information.

Manuscript received February 21, 2019; revised April 9, 2019; accepted May 3, 2019. Date of publication May 8, 2019; date of current version May 24, 2019. This work was supported in part by the National Natural Science Foundation of China under Grant 61605179; in part the Fund of Hubei Key Laboratory of Inland Shipping Technology under Grant NHHY2008002; in part by the Wuhan Science and Technology Bureau under Grant 2018010401011297; and in part by the Fundamental Research Funds for the Central Universities, China University of Geosciences (Wuhan) under Grants 162301132703, G1323511794, and CUG2018JM16. Corresponding author: Tianye Huang (e-mail: tianye_huang@163.com).

Abstract: In this paper, we propose a photonic crystal fiber with broadband ultra-flattened normal dispersion at 2 μm . In this fiber, a subwavelength air hole in the core region and air holes arrangement in the cladding region are used to control the property of dispersion. With optimized design, the dispersion of the proposed ultra-flattened normal dispersion fiber (UNDF) can be kept within -72.4 to -73.15 $\text{ps}\cdot\text{nm}^{-1}\text{km}^{-1}$ from 1750 to 2350 nm wavelength. Benefiting from this advantage, the fiber shows great potential in the applications of coherent supercontinuum (SC) generation and dissipative soliton resonance (DSR) generation in thulium-doped fiber lasers. According to our investigation, coherent SC with 10-dB bandwidth of 238 nm can be obtained by using 50-cm UNDF. Furthermore, by constructing a UNDF-based nonlinear optical loop mirror as a saturable absorber, we specifically investigate the field evolution from dissipative soliton to DSR in passively mode-locked lasers. The proposed UNDF can be a key component for various laser sources in a 2- μm band.

Index Terms: Photonic crystal fiber, fiber lasers, supercontinuum, dissipative soliton resonance.

1. Introduction

With the rapid development of 2 μm band related technology and the huge gain bandwidth (1.8 μm -2.1 μm) provided by thulium-doped fiber (TDF), the 2 μm band has great potential to become the next fiber transmission window [1]–[3]. Furthermore, 2 μm band is safe for human eyes due to its high absorption peak for carbon dioxide and water and it is widely used in various fields.

Supercontinuum (SC) generation and ultrafast pulsed generation are two of the main research hotspots at 2 μm band. SC which features a broadband spectrum is an ideal tool for spectroscopy, optical tomography, sensing, etc. The SC generated in optical fiber is a combined effect between dispersion and nonlinear effects. Typically, it is easier to broaden the optical spectrum by leveraging the anomalous dispersion [4]. However, SC produced in this dispersion regime usually possesses low coherence, which greatly restricts its application in the research fields such as medicine [5], metrology [6] and optical pulse compression [7]. On the contrary, in all-normal dispersion regime, the spectral broadening is mainly dominated by self-phase modulation (SPM) and optical wave breaking (OWB) [8]. Therefore, though SC generated in this regime possesses narrower bandwidth, it enables better pulse to pulse temporal coherence and spectral flatness over the entire output bandwidth compared to its counterpart generated in anomalous dispersion regime [9]. In the past few years, SCs pumped at 2 μm have been theoretically or experimentally demonstrated in various novel fibers with anomalous dispersion [10]–[12]. However, low noise SC originated in pure normal dispersion is still challenge.

Passively mode-locked fiber laser is one of the main methods to produce ultrafast pulses with deterministic repetition rate. Currently, various saturable absorbers (SAs), such as semiconductor saturable absorber mirrors (SESAMs) [13], carbon nanotubes [14]–[16], and graphene [17], have been employed for ultrafast pulse generation. In addition, an effective saturable absorber based on the nonlinear phase shift, is another way to generate mode-locked pulses, such as nonlinear polarization evolution (NPE) [18] and nonlinear optical loop mirror (NOLM) [19]–[21]. Both NPE and NOLM are equivalent to a real SA and sustain high power level. At 2 μm , various fiber lasers have been demonstrated to produce conventional soliton, dissipative soliton (DS), polarization-locked soliton and so on [18], [22]–[24]. Recently, dissipative soliton resonance (DSR) aiming for boosting the single-pulse energy has attracted significant research attention [19]. The characteristic of the DSR phenomenon is that the rectangular pulse width increases with the increase of the cavity power, and the peak power is almost unchanged. In theory, according to the cubic–quintic Ginzburg–Landau equation (CGLE), DSR pulse energy could be increased indefinitely, which is an effective way to obtain high-energy pulses without fluctuations. Most of the previous researches on DSR focused on Ytterbium-doped fiber lasers (YDFLs) and Erbium-doped fiber lasers (EDFLs) operating at 1 μm and 1.5 μm , respectively due to the off-the-shelf high dispersion fibers and optical components at these wavelengths [20], [25]–[27]. For 2 μm , thulium-doped fiber lasers (TDFLs) are also demonstrated to produce DSR pulse by using the ultra-high numerical aperture fiber [21]. However, due to small dispersion of the fiber, the required fiber is relatively long.

As mentioned above, optical fibers with flattened normal dispersion are essential for SC generation with high coherence and DSR generation with compact configuration. Photonic crystal fiber (PCF), whose cladding is replaced by specific periodic structures offers more possibilities to manipulate the features of light propagating inside [28]–[31]. Therefore, fiber dispersion can be more precisely tailored in PCF comparing with traditional step index fibers. Thanks to these advantages, various PCFs are proposed at 2 μm band. For example, tellurite PCF with broadband ultra-flattened dispersion $\sim 61 \text{ ps}\cdot\text{nm}^{-1}\text{km}^{-1}$ can be achieved within wavelength from 2.15 μm to 2.85 μm [32]. Tee et al. presented a near-zero flattened dispersion ZBLAN PCF within 2 μm –3.5 μm [33]. Besides the above-mentioned ones, fibers with flattened large all-normal dispersion can be of great potential for dispersion management at 2 μm .

A slot waveguide can transmit light with a strong field confinement across the subwavelength-scale low-index slot, resulting an effective method to modify the dispersion characteristics. The confinement originates from the large discontinuity of the electric field at a high-index-contrast interface [34]. Recently, the slot effect is transplanted in optical fiber design to tailor the fiber characteristics as well [35], [36]. However, the technique to fabricate a slot in fiber is one of the challenge that need to be faced. Recently, Jiang et al. described the successful fabrication of a ZBLAN PCF with a high air-filling fraction and subwavelength air holes [37], [38]. This kind of improved “stack-and-draw” procedure provides promising support for slot fiber manufacturing.

In this paper, by drawing lessons from the slot waveguide, we proposed a modified PCF by inserting a subwavelength air hole in the core center for tailoring the fiber dispersion. Such hole

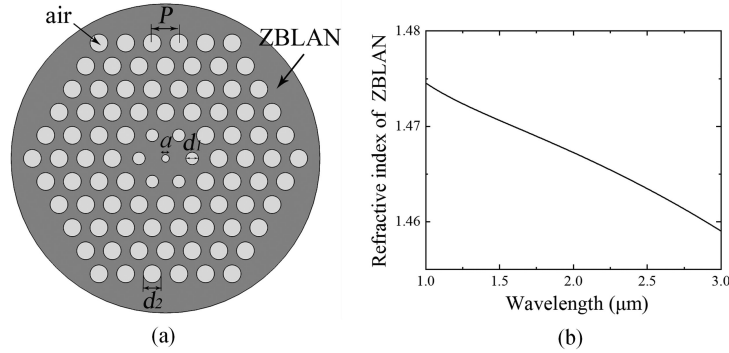


Fig. 1. (a) Cross-section view of the proposed UNDF. (b) Material dispersion of ZBLAN.

confines a large portion of optical fields due to the high index contrast between air and fiber material so that the dispersion can be significantly modified. A broadband ultra-flattened normal dispersion at 2 μm is thus obtained. The fiber is consequently used for highly coherent SC and DSR generation, the dispersion of the proposed ultra-flattened normal dispersion fiber (UNDF) can be kept within $-72.4 \text{ ps}\cdot\text{nm}^{-1}\text{km}^{-1}$ to $-73.15 \text{ ps}\cdot\text{nm}^{-1}\text{km}^{-1}$ from 1750 nm to 2350 nm wavelength. Based on these advantages, we show that such fiber is suitable for coherent SC generation and DSR pulse generation.

2. Fiber Design

2.1 Fiber Structure

The structure of the proposed ultra-flattened normal dispersion fiber (UNDF) is illustrated in Fig. 1(a). The UNDF consists of $\text{ZrF}_4\text{-BaF}_2\text{-LaF}_3\text{-AlF}_3\text{-NaF}$ (ZBLAN) and air holes. The cladding is composed of five layers of air holes with a pitch P . The first layer is used for adjusting the dispersion. The diameters of the first and 2nd–5th layers of air holes are d_1 and d_2 , respectively. Contrary to the conventional PCF structure, there is an air hole with subwavelength scale along the fiber axis to induce the slot effect and its diameter is denoted by a .

The material dispersion of ZBLAN can be calculated from the Sellmeier equation as follows [39]

$$n^2(\lambda) - 1 = \frac{f_1\lambda^2}{(\lambda^2 - \lambda_1^2)} + \frac{f_2\lambda^2}{(\lambda^2 - \lambda_2^2)} \quad (1)$$

with coefficients $\lambda_1 = 0.0954 \mu\text{m}$, $\lambda_2 = 25 \mu\text{m}$, $f_1 = 1.168$ and $f_2 = 2.77$ [40], λ is wavelength of incident light in vacuum. The refractive index of ZBLAN is shown in Fig. 1(b). The group velocity dispersion is defined as

$$D = -\frac{\lambda}{c} \frac{d^2 \text{Re}(n_{\text{eff}})}{d\lambda^2} \quad (2)$$

where c denotes the speed of light in vacuum, $\text{Re}(n_{\text{eff}})$ represents the real part of the mode index at the wavelength of λ . Nonlinear coefficient γ is given by [41]:

$$\gamma = \frac{\omega n_2}{c A_{\text{eff}}} = \frac{2\pi n_2}{\lambda A_{\text{eff}}} \quad (3)$$

where A_{eff} is the mode effective area and n_2 is the nonlinear refractive index with value of $2.1 \times 10^{-20} \text{ m}^2/\text{W}$.

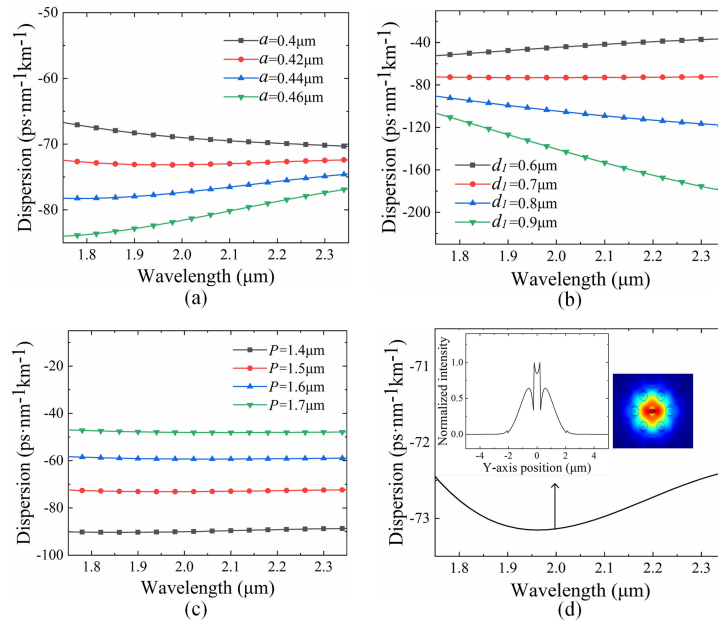


Fig. 2. Dispersion corresponding to the UNDF with different parameters, (a) different a with $d_1 = 0.7 \mu\text{m}$, $P = 1.5 \mu\text{m}$, and $d_2 = 1.0 \mu\text{m}$, (b) different d_1 with $a = 0.42 \mu\text{m}$, $P = 1.5 \mu\text{m}$, and $d_2 = 1.0 \mu\text{m}$, (c) different P with $a = 0.42 \mu\text{m}$, $d_1 = 0.7 \mu\text{m}$, and $d_2 = 1.0 \mu\text{m}$. (d) Dispersion curve of the UNDF with $a = 0.42 \mu\text{m}$, $d_1 = 0.7 \mu\text{m}$, $P = 1.5 \mu\text{m}$, and $d_2 = 1.0 \mu\text{m}$. The insets depict the optical field distributions along the fiber cross-section at the wavelength of 2000 nm.

2.2 Dispersion Optimization

Fig. 1(a) shows the cross-section of the proposed fiber. In order to study the impact of fiber structure on dispersion characteristics, different values of a , d_1 and P are considered, and the results are shown in Fig. 2. The dispersion is normal in the whole scanning wavelength range and becomes larger as a increases, the dispersion curve is the most flattened when $a = 0.42 \mu\text{m}$. The air hole diameter d_1 also demonstrates impacts on the dispersion profile and the dispersion can be further flattened by tailoring d_1 to be $\sim 0.7 \mu\text{m}$, as shown in Fig. 2(b). Different from a and d_1 , the flatness shows less dependence on the pitch P . Nevertheless, the dispersion values can be well-controlled by this parameter with little perturbation to the flatness. As shown in Fig. 2(c), with $a = 0.42 \mu\text{m}$, $d_1 = 0.7 \mu\text{m}$ and $d_2 = 1.0 \mu\text{m}$, the dispersion decreases when P increases from $1.4 \mu\text{m}$ to $1.7 \mu\text{m}$. At the $2 \mu\text{m}$ wavelength, the dispersion is $-48.1 \text{ ps}\cdot\text{nm}^{-1}\text{km}^{-1}$ when $P = 1.7 \mu\text{m}$ and increases to $-90.1 \text{ ps}\cdot\text{nm}^{-1}\text{km}^{-1}$ when $P = 1.4 \mu\text{m}$. From the viewpoint of DSR generation, a large dispersion is desired, which means P should be smaller. However, as d_2/P is larger, the gap between the air holes will be shrank, which may cause the optical fiber to collapse easily during fabrication. Therefore, we choose $a = 0.42 \mu\text{m}$, $d_1 = 0.7 \mu\text{m}$, $d_2 = 1.0 \mu\text{m}$, and $P = 1.5$ in the following analysis. In this condition, the dispersion of the proposed UNDF shows smallest variation and can be kept within $-72.4 \text{ ps}\cdot\text{nm}^{-1}\text{km}^{-1}$ to $-73.15 \text{ ps}\cdot\text{nm}^{-1}\text{km}^{-1}$ from 1750 nm to 2350 nm wavelength, as shown in Fig. 2(d) (note the change in y-axis range). The dispersion slope is $8.2 \times 10^{-4} \text{ ps}\cdot\text{nm}^{-2}\text{km}^{-1}$ and the corresponding nonlinear coefficient is $7.6 \text{ W}^{-1}\text{km}^{-1}$ at 2000 nm. The insets demonstrate the mode profile at 2000 nm, we can see that the electric field at the center air hole is significantly enhanced. It shows that though the refractive index of air is smaller than the fiber material, the discontinuity of electric field vector at the high-index-contrast interface of air and the fiber material still ensure effective field confinement.

3. UNDF-Based Supercontinuum Generation

With all-normal and flattened dispersion, the fiber is investigated for SC generation. The generalized nonlinear Schrödinger equation (GNLSE) is employed to describe the pulse propagation in the UNDF [42], [43]

$$\frac{\partial A}{\partial z} + \frac{\alpha}{2}A - \sum_{k \geq 2} \frac{i^{k+1}}{k!} \beta_k \frac{\partial^k A}{\partial T^k} = i\gamma \left(1 + i\tau_{\text{shock}} \frac{\partial}{\partial T} \right) \left(A(z, T) \int_{-\infty}^{+\infty} R(T') \times |A(z, T - T')|^2 dT' \right) \quad (4)$$

where $A(z, T)$ is the slowly varying complex electrical field envelop at a propagation distance z . α is the linear propagation loss of the UNDF, β_k presenting the dispersion coefficients associated with the Taylor series expansion of the propagation constant $\beta(\omega)$. $R(t)$ is the Raman response function:

$$\begin{aligned} R(t) &= (1 - f_R)\delta(t) + f_R h_R(t) \\ &= (1 - f_R)\delta(t) + f_R \frac{\tau_1^2 + \tau_2^2}{\tau_1 \tau_2} \exp(-t/\tau_2) \sin(t/\tau_1) \Theta(t) \end{aligned} \quad (5)$$

where f_R is the fractional contribution of the delayed Raman response, f_R , τ_1 , τ_2 are related to the fiber material. For ZBLAN, $f_R = 0.1929$, $\tau_1 = 9$ fs, $\tau_2 = 134$ fs [44].

In our simulation, the fiber length is 50 cm. Due to the short length of fiber and the very low loss of ZBLAN fiber at 2 μm band, propagation loss is neglected in the simulation. The nonlinear coefficient γ is 7.6 $\text{W}^{-1}\text{km}^{-1}$ at the pump wavelength of 2000 nm. The dispersion coefficients β_2 to β_{10} are 0.1554 ps^2/m , $-3.2627 \times 10^{-4}\text{ps}^3/\text{m}$, $8.3756 \times 10^{-7}\text{ps}^4/\text{m}$, $-4.1531 \times 10^{-9}\text{ps}^5/\text{m}$, $4.5516 \times 10^{-11}\text{ps}^6/\text{m}$, $-5.45 \times 10^{-13}\text{ps}^7/\text{m}$, $5.766 \times 10^{-15}\text{ps}^8/\text{m}$, $-5.1048 \times 10^{-17}\text{ps}^9/\text{m}$ and $-1.3626 \times 10^{-19}\text{ps}^{10}/\text{m}$ respectively. Hyperbolic secant pulse was selected as the pump pulse with peak power P_0 of 20 kW and full-width at half-maximum (FWHM) of 100 fs. Simulated evolution of spectral and temporal are shown in Fig. 3(a) and (b). It can be seen from the figure that in the evolution of the pulse spectrum with the transmission distance, the spectral broadening is completed within a certain distance ~ 10 cm and dominated by SPM. When the transmission distance increases further, the spectrum is no longer broadened. For example, the spectral spread width at 10 cm and 50 cm are basically the same. This can be attributed to the large dispersion which degrades the pulse peak power quickly and therefore limiting the spectrum broadening. Nevertheless, the 10 dB and 20 dB bandwidth are still as wide as 238 nm and 285 nm respectively.

The modulus of complex degree of coherence is calculated by [45], [46]

$$|g_{12}^{(1)}(\lambda, t_1 - t_2)| = \frac{|\langle E_1^*(\lambda, t_1) E_2(\lambda, t_2) \rangle|}{\sqrt{\langle |E_1(\lambda, t_1)|^2 \rangle \langle |E_2(\lambda, t_2)|^2 \rangle}} \quad (6)$$

where E is the electric field intensity, t is the time measured on the scale of the temporal resolution of the spectrometer used to resolve these spectra. The angle brackets represent the overall average of the independently generated pairs of SC spectra. Fig. 3(c) is the evolutions of coherence properties of the generated SC. The closer to 1, the better the coherence. The generated SC spectra keeps a high degree of coherence because the main driving mechanism in the all-normal dispersion regime is SPM. Additionally, since the dispersion curve is ultra-flattened, the spectra broadening always maintains within the normal dispersion regime ensuring the strong contribution of SPM with high coherence. The influence of the peak power on the SC broadening of the UNDF is plotted in Fig. 3(d). With the peak power increasing from 10 to 40 kW, the output spectra get broadened. The obtained SCs always possess the high spectral flatness.

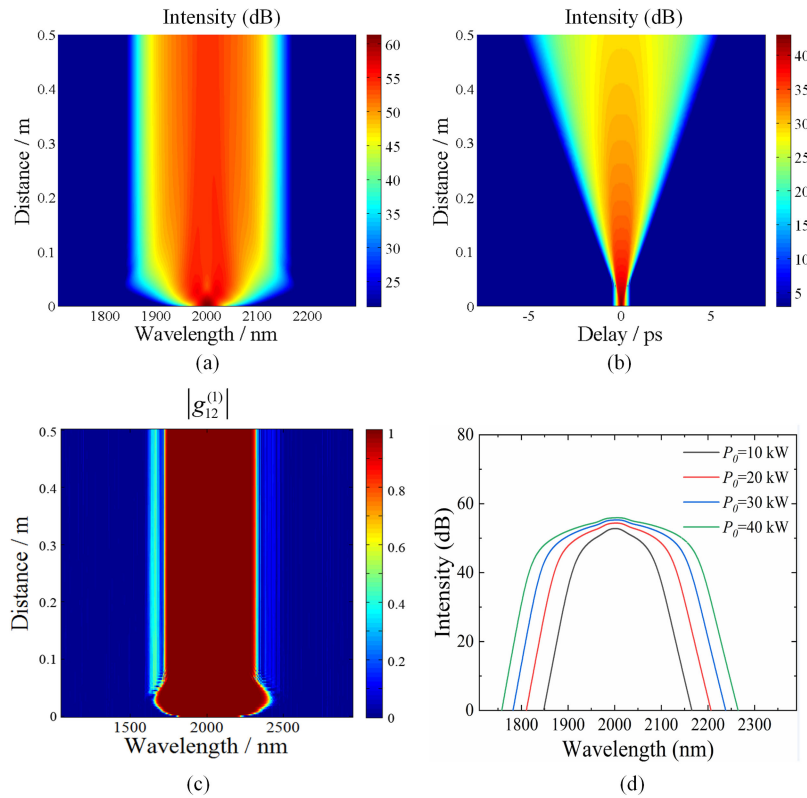


Fig. 3. Simulated evolution of (a) spectral, (b) temporal and (c) complex degree of coherence of SC generation along the entire fiber length in the proposed UNDF. (d) Spectral of the SCs generated with various peak powers.

4. UNDF-Based Fiber Laser for DSR Generation

Recently, the pulse evolution process from dissipative soliton (DS) to DSR in the fiber laser has been analyzed in [47]. However, in this study, the SA is modeled by a Sine-like transmissivity curve, which is not related to practical optical components. For a deeper understanding of the DSR building process in mode-locked fiber lasers, a NOLM constructed by UNDF is placed in a TDFL to play the role as SA and the pulse evolution process is studied in detail.

4.1 Laser Configuration and Numerical Modeling

As shown in Fig. 4(a), the NOLM is formed by an optical coupler (OC) and a section of UNDF. It relies on the interference of the counter-propagating fields, so its saturation power is inversely proportional to the product of splitting ratio and loop length. To achieve low saturation power, we chose a 20:80 coupler and 3-meter-long UNDF. The second-order dispersion parameter of UNDF and nonlinear coefficient γ_{UNDF} are calculated to be $0.155 \text{ ps}^2/\text{m}$ and $7.6 \text{ W}^{-1}\text{km}^{-1}$ at 2000 nm, respectively. The light propagates to the NOLM and is divided into two parts by the 20:80 coupler. Two beams of different intensity pass through the PCF in clockwise and counterclockwise directions, respectively. A_{cw1} and A_{ccw1} are the optical pulse envelope amplitudes of the two different directions divided by the coupler, calculated by:

$$A_{\text{cw1}} = A_0 \times \sqrt{SC} \quad (7)$$

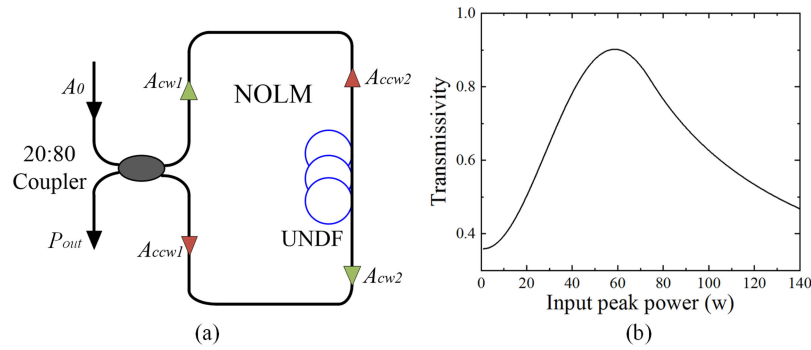


Fig. 4. (a) Structure of NOLM. (b) Transmissivity curve of NOLM.

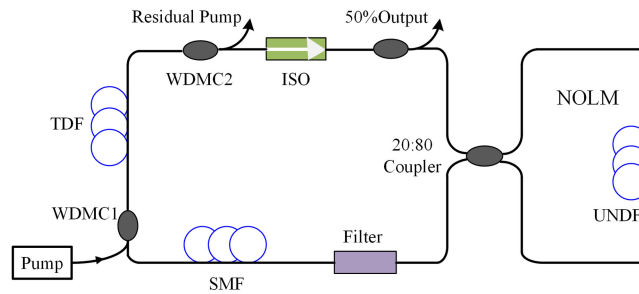


Fig. 5. Schematics of the all-fiber figure-eight passively mode-locked TDFL.

and

$$A_{ccw1} = jA_0 \times \sqrt{1 - SC} \quad (8)$$

where A_0 is the amplitude of the optical pulse envelope input to the coupler, the split coefficient SC of the 20:80 coupler is 0.2. The propagation of pulse in PCF is described as [48]:

$$\frac{\partial A_{cw,ccw}}{\partial z} + \frac{\alpha}{2} A_{cw,ccw} + \frac{i}{2} \beta_2 \frac{\partial^2 A_{cw,ccw}}{\partial t^2} = i\gamma |A_{cw,ccw}|^2 A_{cw,ccw} \quad (9)$$

The optical power after at the output port is calculated by:

$$P_{out} = |A_{cw2} \times \sqrt{SC} + jA_{ccw2} \times \sqrt{1 - SC}|^2 \quad (10)$$

where A_{cw2} and A_{ccw2} represent the two beams after passing through the PCF, and they finally interfere with each other at the output port. The transmissivity T of NOLM can be calculated as follows:

$$T = \frac{P_{peak_out}}{P_{peak_in}} \quad (11)$$

where P_{peak_in} and P_{peak_out} represent the pulse peak power of the input and output NOLM, respectively.

The transmissivity curve of the NOLM is shown in Fig. 4(b). The transmissivity increases as input peak power increment within 0~60 W, showing typical SA property. However, the transmissivity decreases with higher input peak power, demonstrating power clamping effect, which is essential for DSR. It can be seen that the modulation depth is ~ 0.54 and the saturation peak power is ~ 60 W.

The schematics of the all-fiber figure-eight passively mode-locked TDFL is shown in Fig. 5. The right part is the above NOLM. At the left part, the 793 nm pump light is coupled into the fiber via

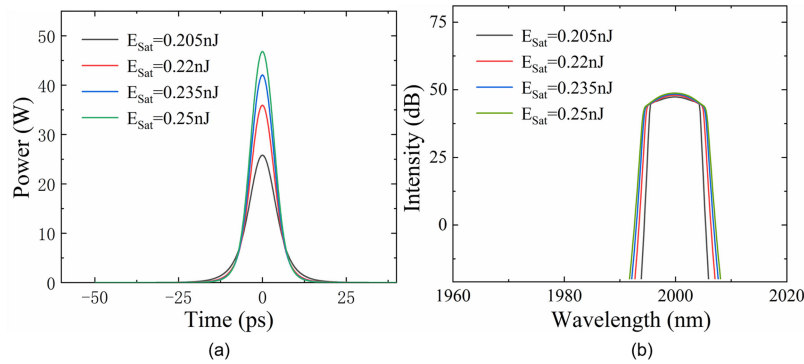


Fig. 6. (a) Temporal waveform and (b) spectrum of DS under different values of E_{Sat} .

a 793/2000 wavelength division multiplexing coupler (WDMC1), the residual pump light is output via the WDMC2. A piece of TDF with 0.5 m length is used as gain medium. Single mode fiber (SMF) has a length of 0.5 m and is denoted for the pigtail of the devices used in the cavity. The second-order dispersion of TDF and SMF are $-0.091 \text{ ps}^2/\text{m}$ and $-0.130 \text{ ps}^2/\text{m}$, respectively. Thus the total cavity dispersion is $\sim 0.356 \text{ ps}^2$. The corresponding nonlinear coefficients are: $\gamma_{SMF} = 1 \text{ W}^{-1}\text{km}^{-1}$ and $\gamma_{TDF} = 3 \text{ W}^{-1}\text{km}^{-1}$, respectively. An isolator ensures the unidirectional operation. The bandwidth of the Gaussian shaped filter is 8 nm. A 50:50 OC is used to extract an output pulse of 2 μm .

In numerical simulation, the propagation of pulse in fiber is described by Ginzburg-Landau equation [48]

$$\frac{\partial A}{\partial z} + \frac{\alpha}{2}A + \frac{i}{2}(\beta_2 + ig(T_2)^2)\frac{\partial^2 A}{\partial t^2} = i\gamma|A|^2A + \frac{1}{2}gA \quad (12)$$

where T_2 denotes the relaxation time, $T_2 = 1/\Delta\omega$, $\Delta\omega = 2\pi c\Delta\lambda/\lambda^2$, where $\Delta\omega$ represents the gain bandwidth, $\Delta\lambda$ means the corresponding FWHM wavelength bandwidth, the gain coefficient g is given by

$$g = \frac{g_0}{1 + E_{Pulse}/E_{Sat}} \quad (13)$$

where E_{Sat} is the gain saturation energy, g_0 is small signal gain at the central wavelength, and E_{pulse} is pulse energy.

4.2 Results and Discussion

To accelerate the convergence of the calculation, initial cavity condition is set to be a 10 ps chirp-free pulse with energy of 100 aJ [30]. The peak power and the central wavelength of the initial pulse are $\sim 9.4 \mu\text{W}$ and 2000 nm, respectively. The value of g_0 is fixed at 2 dB/m. And the gain bandwidth is 40 nm with a Gaussian shape. Under the parameters of the above oscillator, we gradually increase the value of E_{Sat} and observe the change of the output pulse. We first choose four different values of E_{Sat} as 0.205 nJ, 0.22 nJ, 0.235 nJ and 0.25 nJ, the laser output is shown in Fig. 6. Obviously, the cavity delivers optical pulses with steep spectral edges, which is the signature of typical DS. The pulse energy increases from 287.1 pJ to 424.3 pJ as E_{Sat} increases. With the energy increment, the peak power further raises by “over-compression” of the pulse, resulting in little change on FWHM. The spectrum is slightly broadened as well due to self-phase-modulation-(SPM)-induced nonlinear phase shift.

Then, we continue to increase E_{Sat} to 0.3 nJ, 0.4 nJ, 0.5 nJ and 0.6 nJ, see Fig. 7. On the one hand, the peak power increases with larger E_{sat} , which is similar with the DS. On the other hand, higher power part of pulse encounters larger loss induced by NOLM. Therefore, the peak power

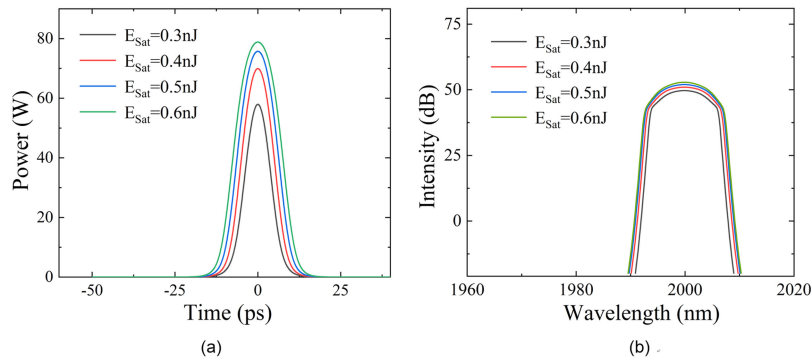


Fig. 7. (a) Temporal waveform and (b) spectrum of TS under different values of E_{Sat} .

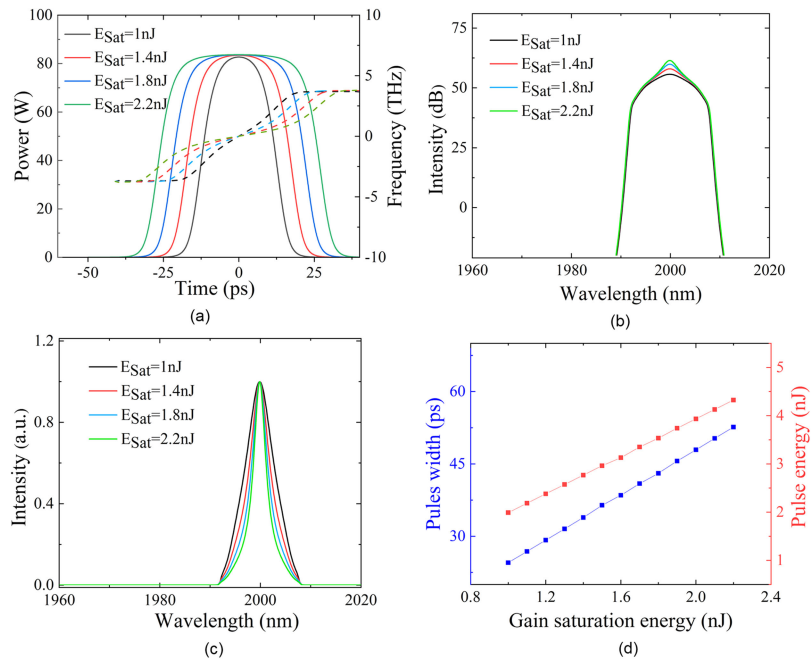


Fig. 8. DSR generation at different values of E_{Sat} . (a) Temporal waveform and chirp, (b) spectra in logarithmic scale, (c) spectra in linear scale, (d) pulse energy (red square) and width (blue square).

increasing speed has been slowed down, and the energy flowing tends to broaden the pulse instead of over-compressing it. The pulse width increases to 8.8 ps, 10.8 ps, 13.0 ps, 15.1 ps, respectively. Since the central portion of the spectrum experiences larger gain than the edge, the amplitude of the central spectrum becomes diverging from the edge, which is more like DSR. Therefore, this operation regime is a transition state (TS), demonstrating both DS and DSR characteristics.

Further increasing the E_{Sat} to 1.0 nJ, 1.4 nJ, 1.8 nJ and 2.2 nJ, the laser is fully turned to generate DSR pulses. As shown in Fig. 8(a), the pulse width gradually increases while its top gradually changes from a bell shape to a rectangle. At the $E_{\text{Sat}} = 2.2$ nJ, the maximum pulse width is 52.6 ps and the pulse energy is calculated to be 4.3 nJ. Peak power is clamped to an almost constant value (82.68 W, 83.38 W, 83.59 W and 83.65 W, respectively), and the pulse becomes rectangular. At this time, reverse SA plays a key role in DSR pulses formation. The peak power of the DSR we observed at the NOLM output is clamped at 60.82 W, which matches well with the transmission property of the UNDF-based NOLM. Meanwhile, the chirp at the pulse peak becomes smaller since

the top of pulse becomes more flattened, which introduces more uniform SPM effect. As the pulse spectra shown in Fig. 8(b) and (c), we found that the newly generated energy locates on the center part of the spectrum while the rectangle part is unchanged. Most energy is stored near the central chirp-free wavelength regime forcing a narrower 3 dB bandwidth. The power scaling relation is drawn in Fig. 8(d) to understand the power characteristics of the DSR laser. Both pulse width and pulse energy monotonically increase indicating the DSR is an efficient way to obtain high-energy pulses.

5. Conclusion

In conclusion, a PCF with broadband ultra-flattened normal dispersion at 2 μm is proposed and investigated. The fiber consists a subwavelength air hole which confines strong optical field in the core center so that the dispersion relation can be effectively tailored. By selecting the appropriate center air hole diameter and carefully arranging the cladding air hole distribution, the proposed UNDF demonstrates large flattened dispersion $\sim -73 \text{ ps}\cdot\text{nm}^{-1}\text{km}^{-1}$ in the wavelength range from 1750 nm to 2350 nm. The applications of this fiber for SC and DSR soliton generation are investigated further. The generated SC spectrum keeps a high degree of coherence with 10-dB bandwidth more than 200 nm. By inserting the UNDF in an all-fiber figure-eight mode-locked TDFL, the pulse evolution process from DS to DSR is well studied. The UNDF can be employed for both linear and nonlinear applications in the emerging 2 μm band.

References

- [1] H. Zhang *et al.*, "100 Gbit/s WDM transmission at 2 μm : transmission studies in both low-loss hollow core photonic bandgap fiber and solid core fiber," *Opt. Exp.*, vol. 23, no. 4, pp. 4946–4951, Feb. 2015.
- [2] M. N. Petrovich *et al.*, "Demonstration of amplified data transmission at 2 microns in a low-loss wide bandwidth hollow core photonic bandgap fiber," *Opt. Exp.*, vol. 21, no. 23, pp. 28559–28569, Nov. 2013.
- [3] H. Zhang *et al.*, "Dense WDM transmission at 2 μm enabled by an arrayed waveguide grating," *Opt. Lett.*, vol. 40, no. 14, pp. 3308–3311, Jul. 2015.
- [4] A. Abeeluck and C. Headley, "Continuous-wave pumping in the anomalous- and normal-dispersion regimes of nonlinear fibers for supercontinuum generation," *Opt. Lett.*, vol. 30, no. 23, pp. 61–63, 2005.
- [5] J. Yi, S. Chen, X. Shu, A. Fawzi, and H. Zhang, "Human retinal imaging using visible-light optical coherence tomography guided by scanning laser ophthalmoscopy," *Opt. Exp.*, vol. 6, pp. 3701–3713, 2015.
- [6] T. Udem, R. Holzwarth, and T. W. Hänsch, "Optical frequency metrology," *Nature*, vol. 416, pp. 233–237, 2002.
- [7] J. Dudley and S. Coen, "Fundamental limits to few-cycle pulse generation from compression of supercontinuum spectra generated in photonic crystal fiber," *Opt. Exp.*, vol. 12, pp. 2423–2428, 2004.
- [8] L. Liu *et al.*, "Coherent mid-infrared supercontinuum generation in all-solid chalcogenide microstructured fibers with all-normal dispersion," *Opt. Lett.*, vol. 41, no. 2, pp. 392–395, Jan. 2016.
- [9] G. Stepniwski *et al.*, "Broadband supercontinuum generation in normal dispersion all-solid photonic crystal fiber pumped near 1300 nm," *Laser Phys. Lett.*, vol. 11, Mar. 2014, Art. no. 055103.
- [10] R. Ahmad, M. Komanec, and S. Zvanovec, "Circular lattice photonic crystal fiber for Mid-IR supercontinuum generation," *IEEE Photon. Technol. Lett.*, vol. 28, no. 23, pp. 2736–2739, Dec. 2016.
- [11] J. Swiderski, M. Michalska, and P. Grzes, "Broadband and top-flat mid-infrared supercontinuum generation with 3.52 W time-averaged power in a ZBLAN fiber directly pumped by a 2- μm mode-locked fiber laser and amplifier," *Appl. Phys. B*, vol. 124, 2018, Art. no. 152.
- [12] M. Michalska, J. Mikolajczyk, J. Wojtas, and J. Swiderski, "Mid-infrared, super-flat, supercontinuum generation covering the 2–5 μm spectral band using a fluorindate fiber pumped with picosecond pulses," *Sci. Rep.*, vol. 6, 2016, Art. no. 39138.
- [13] U. Keller, "Recent developments in compact ultrafast lasers," *Nature*, vol. 424, pp. 831–838, 2003.
- [14] X. Liu and Y. Cui, "Revealing the behavior of soliton buildup in a mode-locked laser," *Adv. Photon.*, vol. 1, no. 1, 2019, Art. no. 016003.
- [15] X. Liu *et al.*, "Versatile multi-wavelength ultrafast fiber laser mode-locked by carbon nanotubes," *Sci. Rep.*, vol. 3, 2013, Art. no. 2718.
- [16] X. Liu, X. Yao, and Y. Cui, "Real-time observation of the buildup of soliton molecules," *Phys. Rev. Lett.*, vol. 121, Jul. 2018, Art. no. 023905.
- [17] F. Bonaccorso, Z. Sun, T. Hasan, and A. C. Ferrari, "Graphene photonics and optoelectronics," *Nature Photon.*, vol. 4, pp. 611–622, 2010.
- [18] C. Gao, Z. Wang, H. Luo, and L. Zhan, "High energy all-fiber Tm-doped femtosecond soliton laser mode-locked by nonlinear polarization rotation," *J. Lightw. Technol.*, vol. 35, no. 14, pp. 2988–2993, Jul. 2017.
- [19] J. Yang *et al.*, "Observation of dissipative soliton resonance in a net-normal dispersion figure-of-eight fiber laser," *IEEE Photon. J.*, vol. 5, no. 3, Jun. 2013, Art. no. 1500806.

- [20] S. Wang, Q. Ning, A. Luo, Z. Lin, Z. Luo, and W. Xu, "Dissipative soliton resonance in a passively mode-locked figure-eight fiber laser," *Opt. Exp.*, vol. 21, pp. 2402–2407, 2013.
- [21] Y. Xu *et al.*, "Dissipative soliton resonance in a wavelength-tunable thulium-doped fiber laser with net-normal dispersion," *IEEE Photon. J.*, vol. 7, no. 3, Jun. 2015, Art. no. 1502007.
- [22] H. Li, J. Liu, Z. Cheng, J. Xu, F. Tan, and P. Wang, "Pulse-shaping mechanisms in passively mode-locked thulium-doped fiber lasers," *Opt. Exp.*, vol. 23, pp. 6292–6303, 2015.
- [23] W. Zhou *et al.*, "Stable passively harmonic mode-locking dissipative pulses in 2 μm solid-state laser," *Opt. Exp.*, vol. 25, pp. 1815–1823, 2017.
- [24] P. Wang, X. Xiao, and C. Yang, "Quantized pulse separations of phase-locked soliton molecules in a dispersion-managed mode-locked Tm fiber laser at 2 μm ," *Opt. Lett.*, vol. 42, pp. 29–32, 2017.
- [25] D. Li, D. Shen, L. Li, D. Tang, L. Su, and L. Zhao, "Internal polarization dynamics of vector dissipative-soliton-resonance pulses in normal dispersion fiber lasers," *Opt. Lett.*, vol. 43, pp. 1222–1225, 2018.
- [26] L. Liu *et al.*, "Wave-breaking-free pulse in an all-fiber normal-dispersion Yb-doped fiber laser under dissipative soliton resonance condition," *Opt. Exp.*, vol. 21, pp. 27087–27092, 2013.
- [27] D. J. Richardson, R. I. Laming, D. N. Payne, V. Matsas, and M. W. Phillips, "Selfstarting, passively modelocked erbium fiber ring laser based on the amplifying Sagnac switch," *Electron. Lett.*, vol. 27, no. 6, pp. 542–544, 1991.
- [28] J. C. Knight, "Photonic crystal fibers," *Nature*, vol. 424, pp. 847–851, 2003.
- [29] J. C. Knight, J. Arriaga, T. A. Birks, A. Ortigosa-Blanch, W. J. Wadsworth, and P. S. J. Russell, "Anomalous dispersion in photonic crystal fiber," *IEEE Photon. Technol. Lett.*, vol. 12, no. 7, pp. 807–809, Jul. 2000.
- [30] Y. Gao *et al.*, "Design of ultra large normal dispersion ZBLAN photonic crystal fiber and its application in Mid-IR ultra short fiber lasers," *IEEE Photon. J.*, vol. 10, no. 6, Dec. 2018, Art. no. 1504509.
- [31] D. Ghosh, S. Roy, M. Pal, A. Pal, and S. K. Bhadra, "Index-guided photonic crystal fibers: study of fiber drawing parameters," *J. Opt.*, vol. 37, pp. 72–77, 2008.
- [32] T. Huang, P. Huang, Z. Cheng, J. Liao, X. Wu, and J. Pan, "Design and analysis of a hexagonal tellurite photonic crystal fiber with broadband ultra-flattened dispersion in mid-IR," *Optik*, vol. 167, pp. 144–149, 2018.
- [33] D. C. Tee, N. Tamchek, and C. H. Raymond Ooi, "Numerical modeling of the fundamental characteristics of ZBLAN photonic crystal fiber for communication in 2–3 μm midinfrared region," *IEEE Photon. J.*, vol. 8, no. 2, Apr. 2016, Art. no. 4500713.
- [34] V. Almeida, Q. Xu, C. Barrios, and M. Lipson, "Guiding and confining light in void nanostructure," *Opt. Lett.*, vol. 29, pp. 1209–1211, 2004.
- [35] T. Huang, J. Liao, S. Fu, M. Tang, P. Shum and D. Liu, "Slot spiral silicon photonic crystal fiber with property of both high birefringence and high nonlinearity," *IEEE Photon. J.*, vol. 6, no. 3, Jun. 2014, Art. no. 2200807.
- [36] J. Liao, Y. Xie, X. Wang, D. Li, and T. Huang, "Ultra-flattened nearly-zero dispersion and ultrahigh nonlinear slot silicon photonic crystal fibers with ultrahigh birefringence," *Photon. Nanostruct.—Fundam. Appl.*, vol. 25, pp. 19–24, 2017.
- [37] X. Jiang *et al.*, "Deep-ultraviolet to mid-infrared supercontinuum generated in solid-core ZBLAN photonic crystal fibre," *Nature Photon.*, vol. 9, pp. 133–137, 2015.
- [38] X. Jiang *et al.*, "Supercontinuum generation in ZBLAN glass photonic crystal fiber with six nanobore cores," *Opt. Lett.*, vol. 41, pp. 4245–4248, 2016.
- [39] K. Saitoh and M. Koshiba, "Full-vectorial imaginary-distance beam propagation method based on finite element scheme: Application to photonic crystal fibers," *IEEE J. Quantum Electron.*, vol. 38, no. 7, pp. 927–933, Jul. 2002.
- [40] Q. Yang, L. Miao, G. Jiang, and C. Zhao, "Modeling the broadband mid-Infrared dispersion compensator based on ZBLAN microfiber," *IEEE Photon. Technol. Lett.*, vol. 28, no. 7, pp. 728–731, Apr. 2016.
- [41] J. F. Liao, T. Y. Huang, Z. Z. Xiong, F. G. Kuang, and Y. M. Xie, "Design and analysis of an ultrahigh birefringent nonlinear spiral photonic crystal fiber with large negative flattened dispersion," *Optik*, vol. 135, pp. 42–49, 2017.
- [42] W. Qi, X. Huang, D. Ho, S. Yoo, K. T. Yong, and F. Luan, "Microstructured inline optical fiber structure for dispersion control and coherent supercontinuum generation," *IEEE Photon. J.*, vol. 8, no. 3, Jun. 2016, Art. no. 7101209.
- [43] J. M. Dudley, "Supercontinuum generation in photonic crystal fiber," *Rev. Modern Phys.*, vol. 78, pp. 1135–1184, 2006.
- [44] L. Liu, G. Qin, Q. Tian, D. Zhao, and W. Qin, "Numerical investigation of mid-infrared supercontinuum generation up to 5 μm in single mode fluoride fiber," *Opt. Exp.*, vol. 19, pp. 10041–10048, May 2011.
- [45] G. Genty, M. Surakka, J. Turunen, and A. Friberg, "Complete characterization of supercontinuum coherence," *J. Opt. Soc. Am. B*, vol. 28, pp. 2301–2309, 2011.
- [46] J. M. Dudley and S. Coen, "Coherence properties of supercontinuum spectra generated in photonic crystal and tapered optical fibers," *Opt. Lett.*, vol. 27, pp. 1180–1182, 2002.
- [47] Z. Cheng, H. Li, and P. Wang, "Simulation of generation of dissipative soliton, dissipative soliton resonance and noise-like pulse in Yb-doped mode-locked fiber lasers," *Opt. Exp.*, vol. 23, pp. 5972–5981, 2015.
- [48] X. Wu, Z. Wu, T. Huang, B. Chen, K. Ren, and S. Fu, "All-optical actively mode-locked fiber laser at 2- μm based on inter-band modulation," *IEEE Photon. J.*, vol. 9, no. 5, Oct. 2017, Art. no. 1505908.